Supporting Information

Cation-anion Double Hydrolysis Derived Layered Single Metal Hydroxide Superstructure for Boosted Supercapacitive Energy Storage

C. D. Gu[1], X. Ge, X.L. Wang, J.P. Tu

State Key Laboratory of Silicon Materials, Key Laboratory of Advanced Materials and Applications for Batteries of Zhejiang Province and School of Materials Science and Engineering, Zhejiang University, Hangzhou 310027, China.

[1] *Corresponding Author
Tel./fax.: +86 571 87952573
E-mail addresses: cdgu@zju.edu.cn (C. D. Gu)

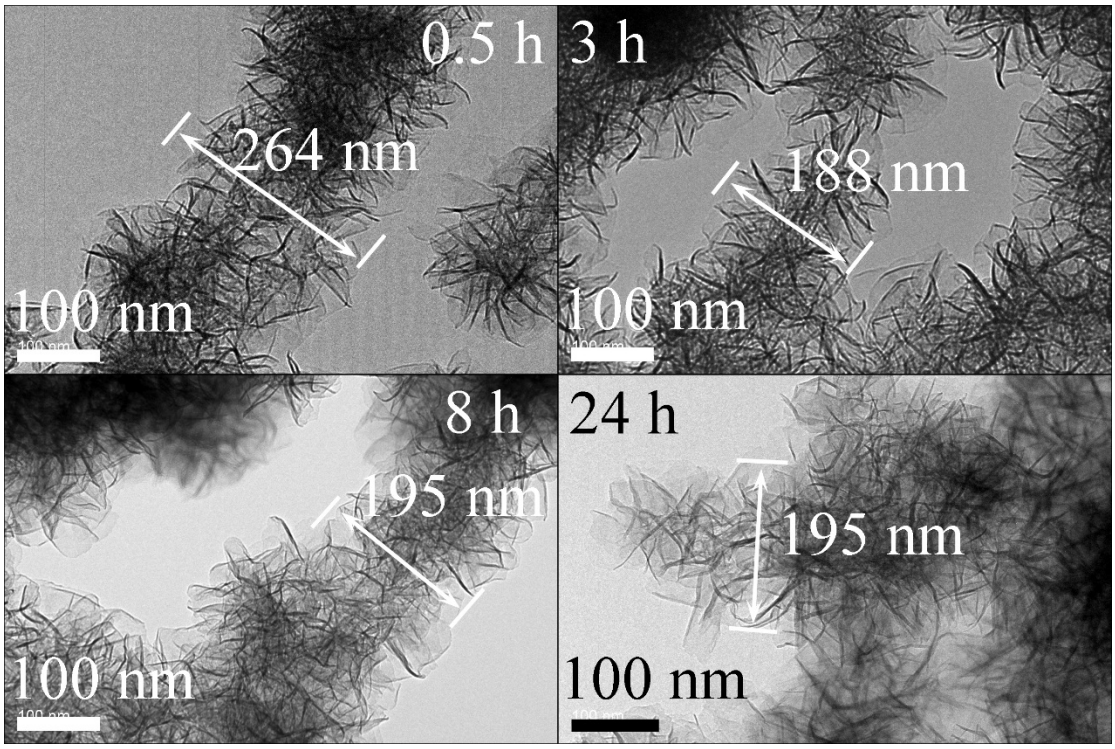

Figure S1 Time dependent experiment showing the growth process of 3D-ICHA α-$Ni(OH)_2$.

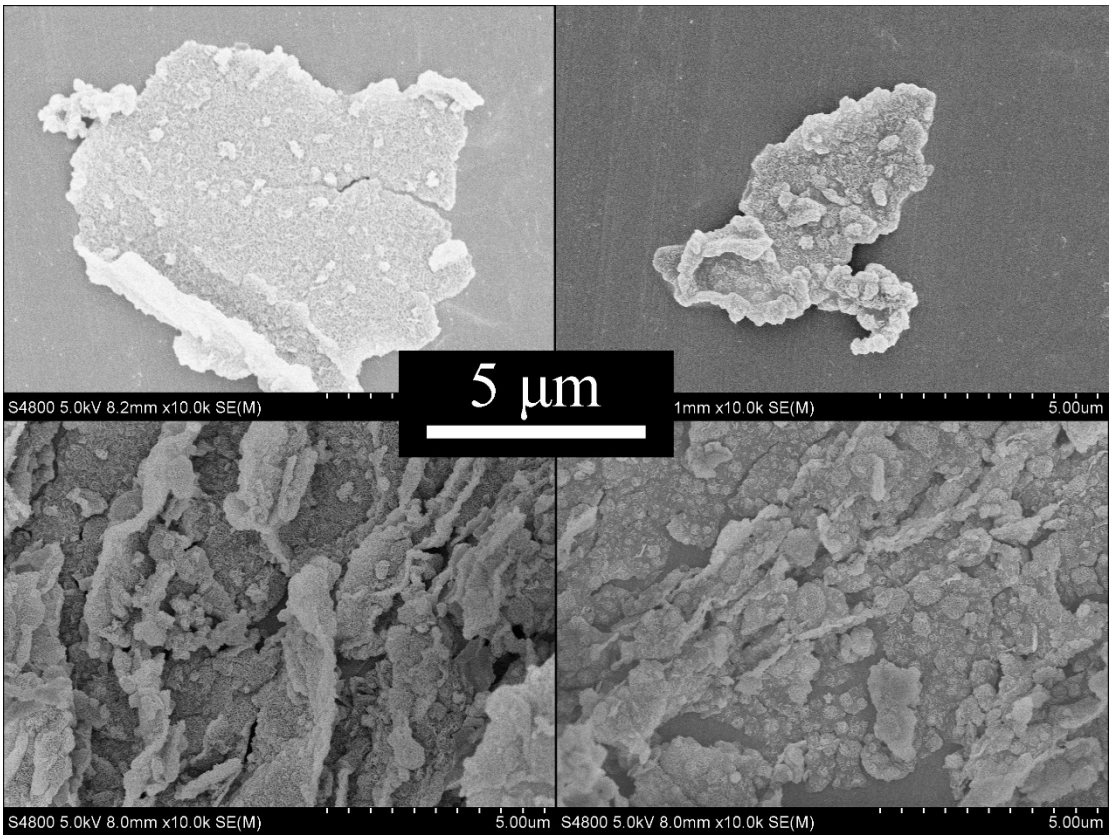

Figure S2 More SEM images of SOS α-$Ni(OH)_2$. The non-uniform nature of the lateral size of the sheet in the substrate can be observed.

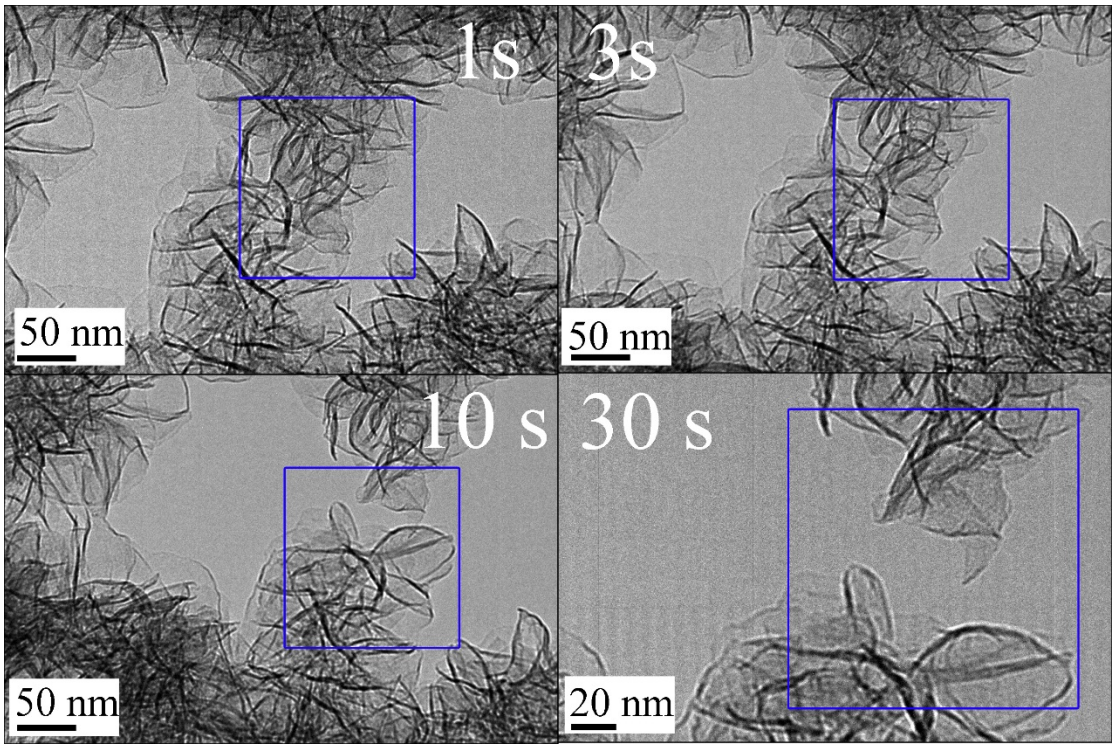

Figure S3 A weakly connected region of 3D-ICHA α-$Ni(OH)_2$ is torn apart by electron beam radiation, while the building blocks weren't torn apart.

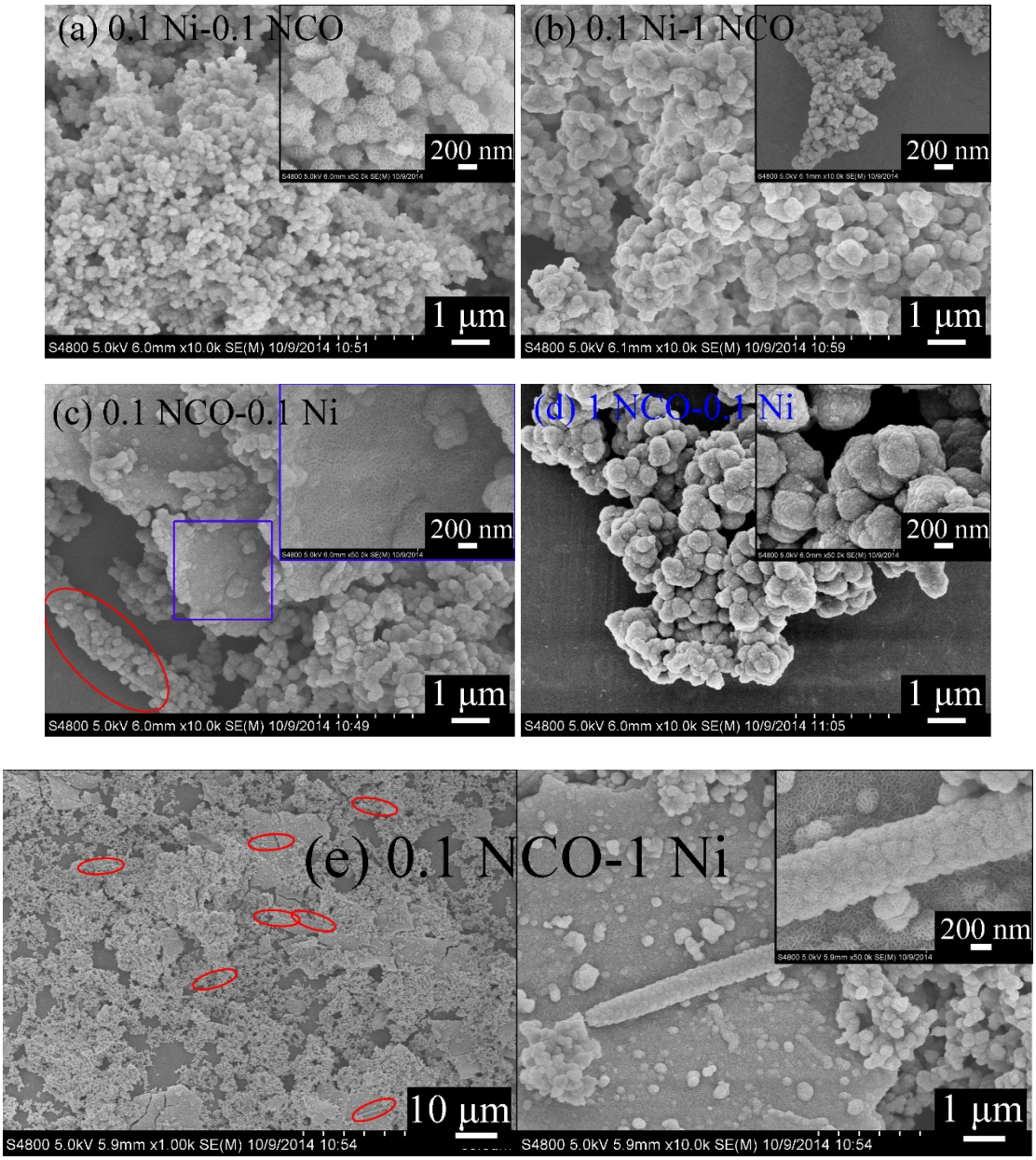

Figure S4 Influence of pumping method and concentration on the assembly behavior of α-$Ni(OH)_2$. In (a) and (b) Ni^{2+} was pumped into NCO^-, while the concentration is different (a: 0.1 M Ni-0.1 NCO, b: 0.1 M Ni-1 NCO). In (c-e) NCO^- was pumped into Ni^{2+} (c: 0.1 NCO-0.1 Ni , d: 1 NCO-0.1 Ni, e: 0.1 NCO-1 Ni). We highlight the existance of sheet-on-rod α-$Ni(OH)_2$ with elliptic red marks.

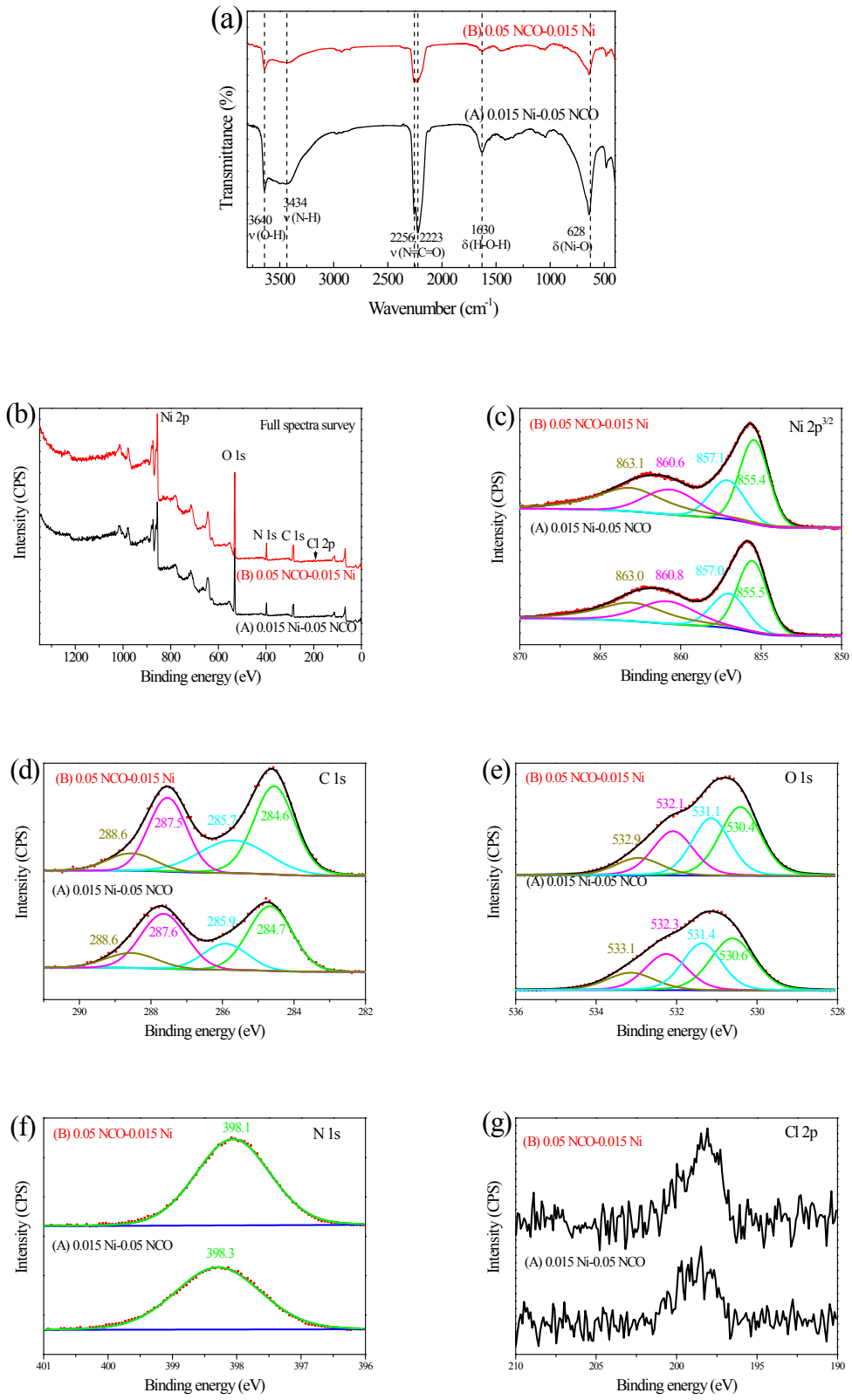

Figure S5 FTIR (a) and XPS (b-g) spectra of 3D-ICHA α-$Ni(OH)_2$ and SOS α-$Ni(OH)_2$.

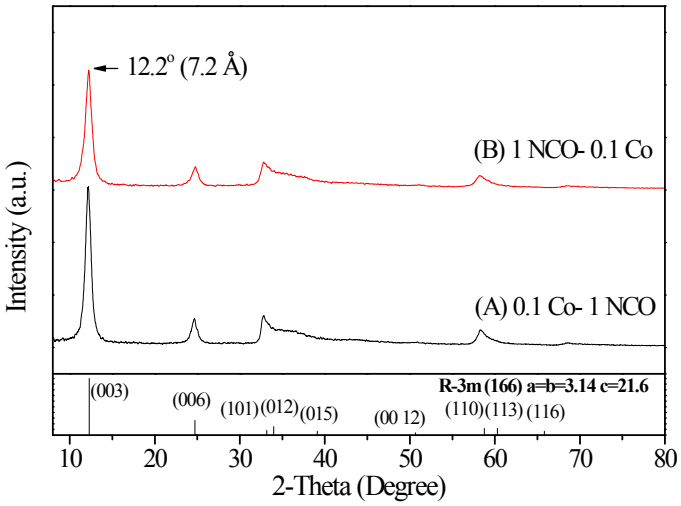

Figure S6 XRD patterns of (A) 0.1 Co- 1 NCO and (B) 0.1 NCO- 1 Co.

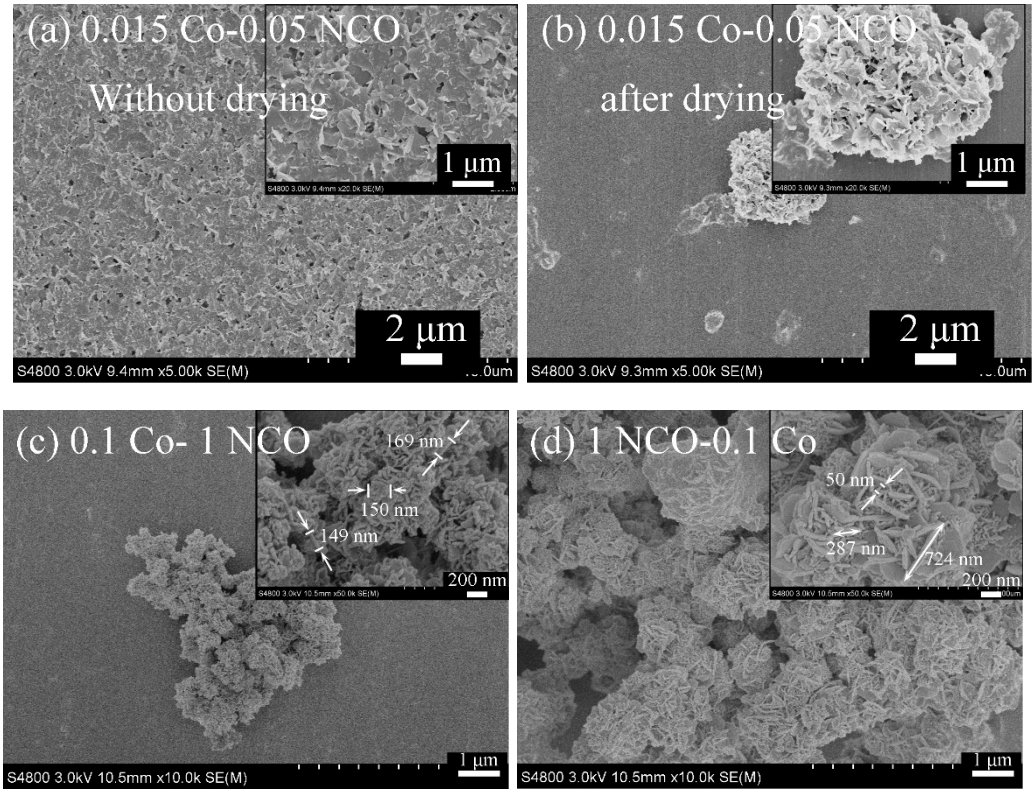

Figure S7 SEM images of (a) 0.015 Co-0.05 NCO sampled without drying, (b) 0.015 Co-0.05 NCO sampled after drying and redispered in ethonal, (c) 0.1 Co- 1 NCO and (d) 1 NCO- 0.1 Co.

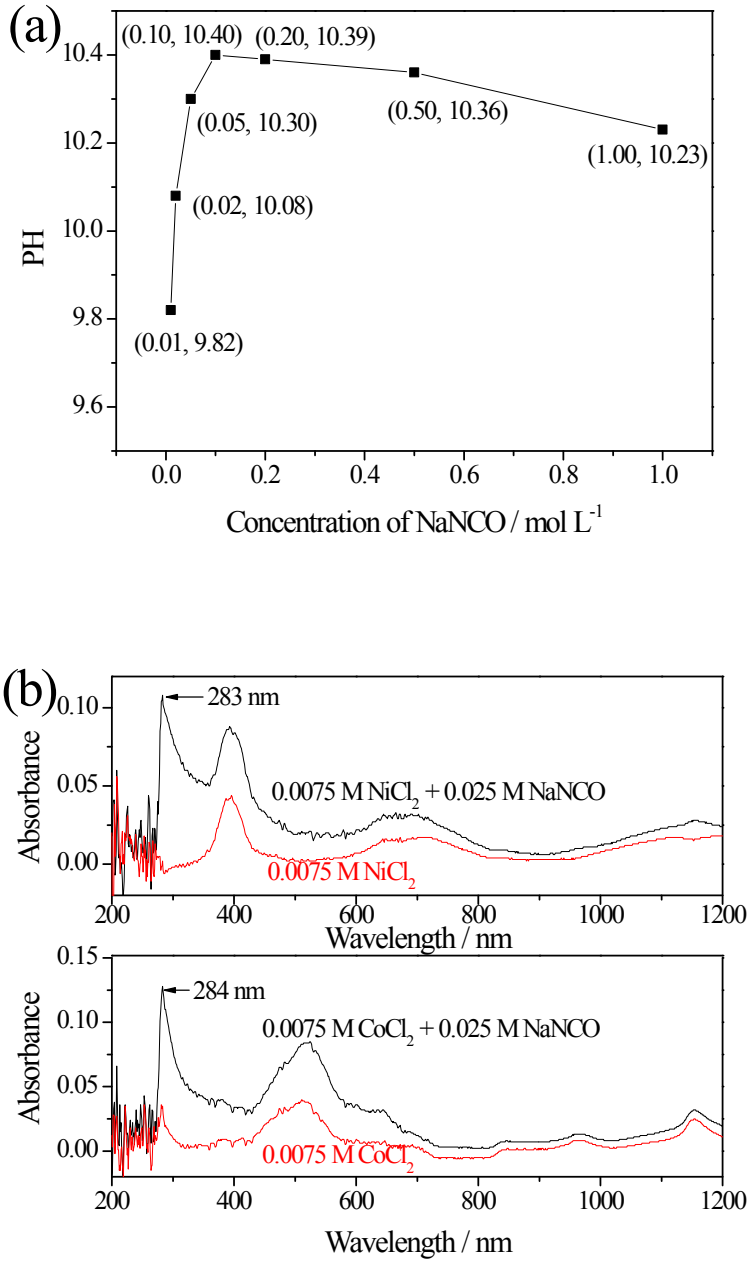

Figure S8 (a) The pH value of the aqueous solution of NaNCO with different concentrations. (b) UV-Vis spectra of aqueous solution containing bare metal ions (Ni^{2+} or Co^{2+}) or metal ions mixed with NCO^-.

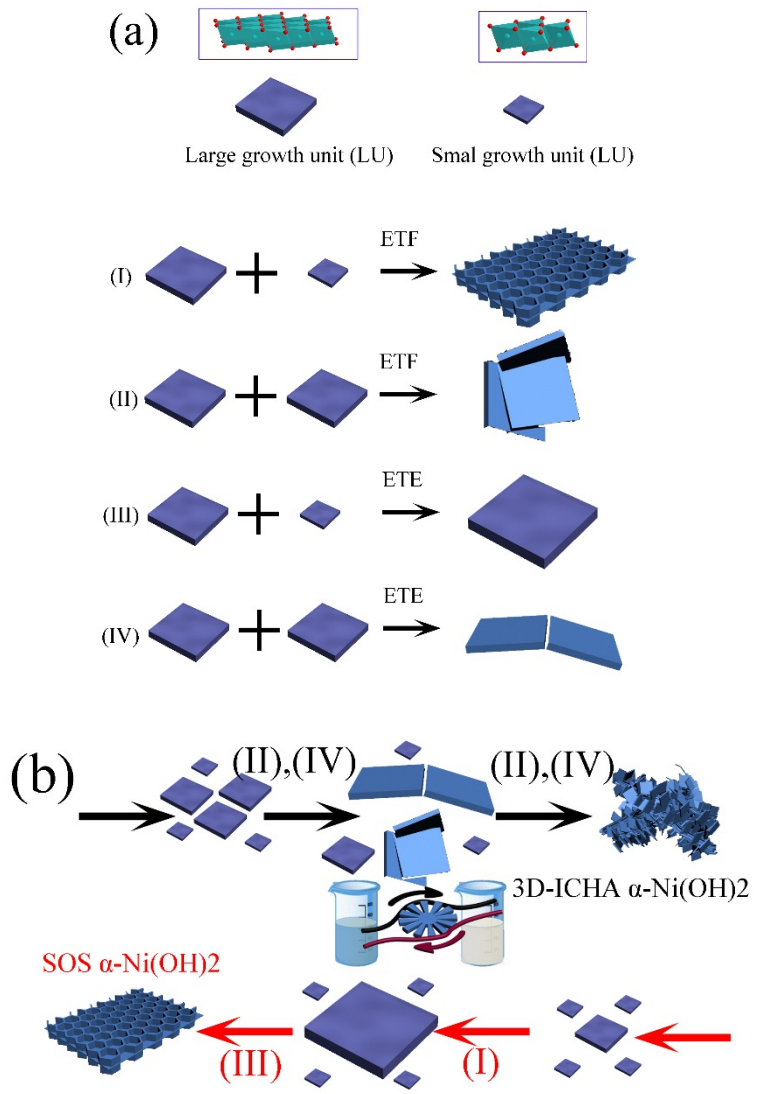

Figure S9 (a) shows the main interaction modes (edge-to-edge detoned as ETE and edge-to-face denoted as ETF) of small growth units (SM) and large growth units (LU). (b) shows the formation process of 3D-ICHA α-$Ni(OH)_2$ and SOS α-$Ni(OH)_2$.

Double hydrolysis mechanism for the assembly of LSHs.

The aqueous solution of NaNCO with concentrations ranging from 0.01-1 M has a narrow pH value distribution within 9.8-10.4, which is favorable for the formation of $Ni(OH)_2$ or $Co(OH)_2$. Meanwhile, the precipitation of α-phase metal hydroxides should be attributed to the formation of $Ni_4(OH)_4^{4+}$ or $Co_4(OH)_4^{4+}$ tetramers and further condensation based on *minimal structural change*.[1] $Ni_4(OH)_4^{4+}$ or $Co_4(OH)_4^{4+}$ is supposed to serve as the basic growth unit in solution to grow 2D α-type metal hydroxides as building blocks for a series of anisotropic assembly structures.[2] Moreover, the hydrolysis reaction kinetics should be highly dependent on the mixing modes of NaNCO and metal ions, which will determine the morphologies of products (see Figure 3, Figure 6, Figure S1-S4 and Figure S7).

We first define two kinds of 2D building blocks as small unit (SU) and large unit (LU).[2] The SU can not nucleate out from the solution but could adhere to existing crystal nuclei, which is also named as "pre-nucleation" clusters in some literatures.[3-5] The LU can directly precipitate out from the solution. Those developed micrometer sheets are also categorized as LU. One main difference between SU and LU during interaction is that SU is more likely to reorganize its structure after being attached to another growth unit. For this protocol, we can simply consider the competing edge-to-edge (ETE) and edge-to-face (ETF) interactions of 2D building blocks. The ETE and ETF interactions are also widely noticed to determine the assembly process of other 2D growth unites.[6, 7] As shown in Figure S9a, there should be four kinds of basic assembly behavior: ETF between LU and LU, ETF between LU and SU, ETE between LU and LU, ETE between LU and SU. As a representative example, the formation process of 3D-ICHA α-$Ni(OH)_2$ and SOS α-$Ni(OH)_2$ is shown in Figure S9b. With a higher reaction kinetics (i.e., metal ion solution is introduced into NaNCO solution), nucleation is fast and large amount of hydroxides would precipitate, interact and assemble. The instant depletion of Ni^{2+} would leave few SU to form, thus hindering the growth of LU through mode (III). The obtained α-$Ni(OH)_2$ has a relatively smaller size and lower crystallinity as indicated above. Large amounts of LU would directly interact through mode (II) and (IV) to form clusters. Due to higher reaction kinetics and fast assembly process, these clusters are ready to twist with each other and form 3D-ICHA structures (Figure 3a and 3c). On the other hand, when aqueous solution of NaNCO is gradually added into Ni^{2+} solution which delivers

lower hydrolysis reaction kinetics, the kinetics would gradually increase until nucleation. Once nucleation happens, the kinetics immediately decreases due to the consumption of nutrients. Then the kinetics would be kept at a stage where the formation of SU is dominated and the SU has enough time to reorganize. When the SU interact with initially precipitated LU in mode (III), the LU could grow into larger LU. On the surface of the larger LU, further precipitation and organization of SU in mode (I) would lead to the formation of SOS structure (Figure 3b and 3d). The formation process of the α-$Co(OH)_2$ nanostructures shown in this work can also be understood according to the proposed assembly mechanism.

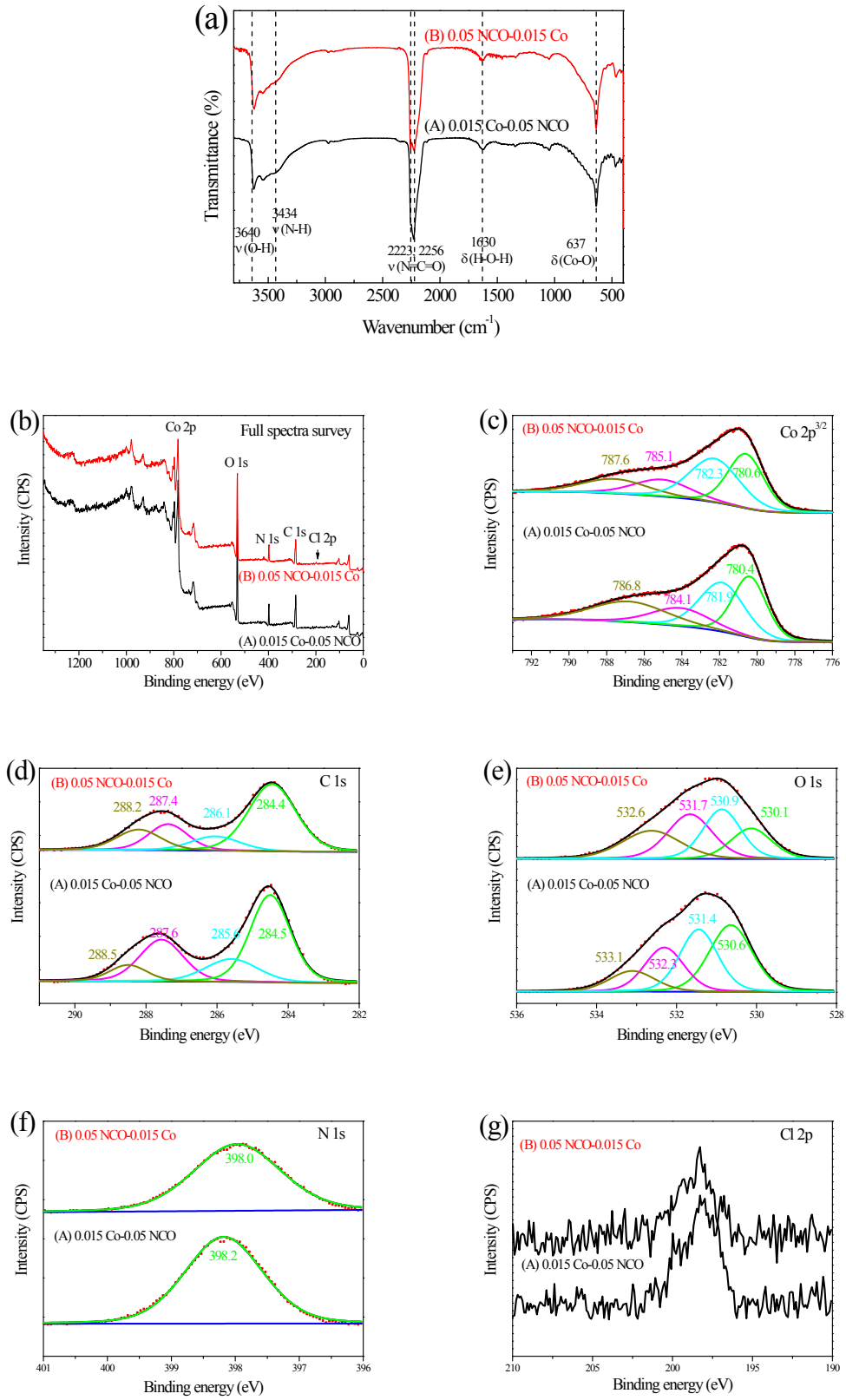

Figure S10 FTIR (a) and XPS (b-g) of 0.015 Co- 0.05 NCO and 0.015 Co- 0.05 NCO.

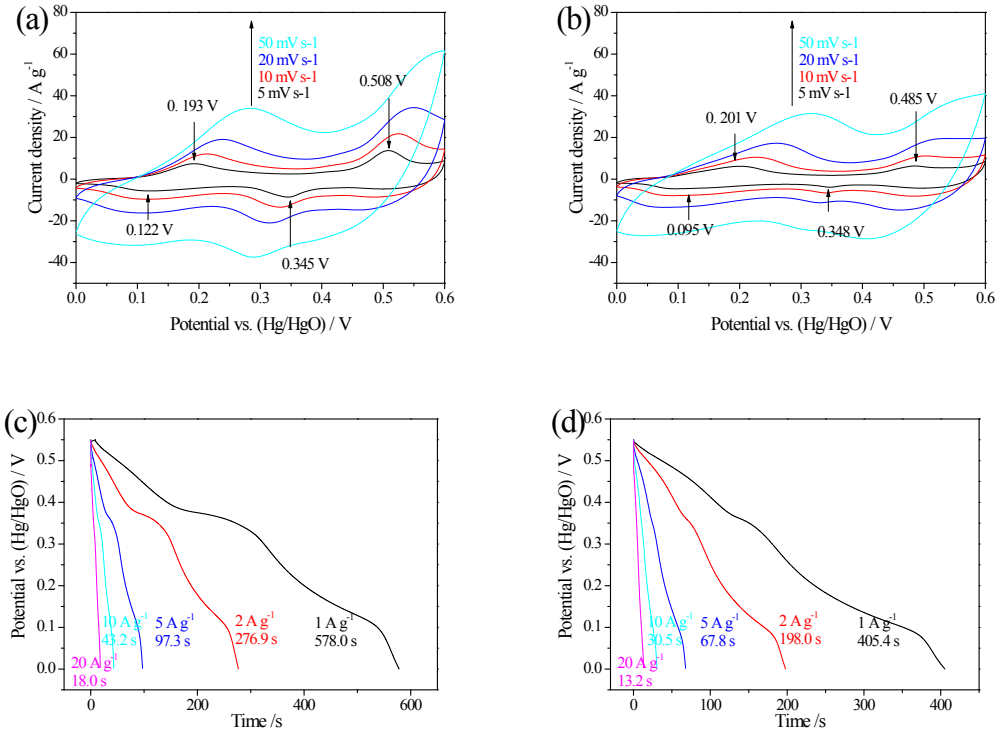

Figure S11 (a and c) show the CV and choronopotentiometry curves of LP α-$Co(OH)_2$; (b and d) show the CV and choronopotentiometry curves of WDS α-$Co(OH)_2$.

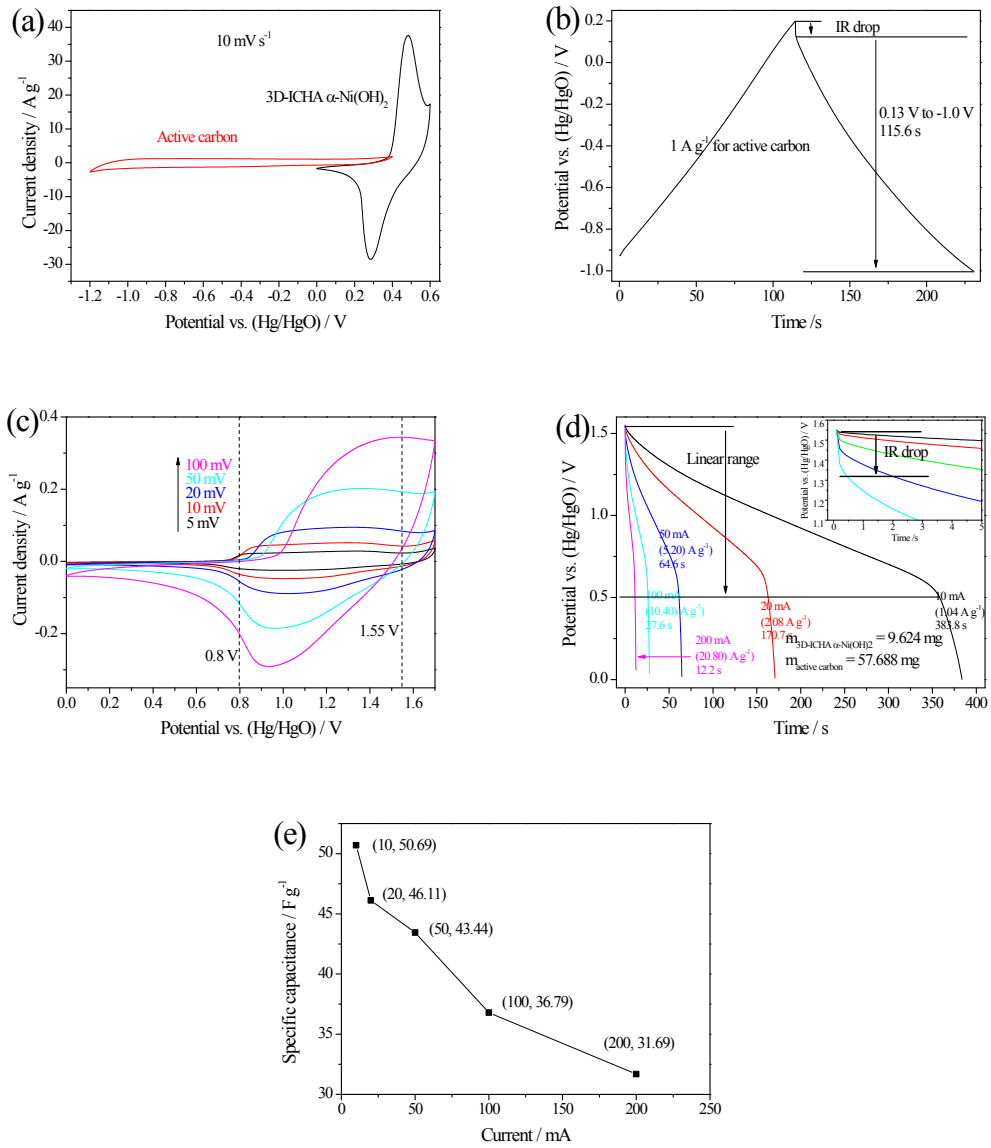

Figure S12 (a and b) show the CV (10 mV s^{-1}) and chronopotentiometry curves (1 A g^{-1}) of actived carbon and 3D-ICHA α-$Ni(OH)_2$ at 10 mV s^{-1}. (c-e) show the electrochemical behavior of a high-loading full capacitor with excessive actived carbon (9.624 mg 3D-ICHA α-$Ni(OH)_2$ and 57.688 mg actived carbon). (c) gives the CV curves. (d) shows the chronopotentiometry curves of the asymmetric supercapacitor.. (e) gives the specific capacitance based on the active materials on both electrodes.

Table S1 Literature comparison of supercapacitor performance based on $Ni(OH)_2$. In particular, papers reporting powder-based α-$Ni(OH)_2$ are exhaustively collected. The parameters which are superior, comparable or inferior to those of 3D-ICHA α-$Ni(OH)_2$ are highlighted as blue, green or red, respectively.

Phase	Structure	Specific surface area / $m^2\ g^{-1}$	Specific charge storage capacity / $C\ g^{-1}$	Cycling retention	Loading mass	Refs.
α-$Ni(OH)_2$	**3-D inter-connected Hierarchical assembly**	**320.2**	**653.1 (1 A g^{-1}) 619.2 (2 A g^{-1}) 554.5 (5 A g^{-1}) 499.0 (10 A g^{-1}) 406.0 (20 A g^{-1})**	**86.2 %（20000 cycles） 90.6 % (5000 cycles) 10 A g^{-1}**	**1.5± 0.3 mg**	**This work**
α-$Ni(OH)_2$	**Sheet-on-sheet**	**115.6**	**289.4 (1 A g^{-1}) 249.6 (2 A g^{-1}) 241.5 (5 A g^{-1}) 209.0 (10 A g^{-1}) 166.0 (20 A g^{-1})**	**98.6 % (5 A g^{-1}, 5000 cycles)**	**1.5 ± 0.3 mg**	**This work**
α-$Ni(OH)_2$	Fish-scale like	\	\	95 % (10 mA, 200 cycles)	\	8
α-$Ni(OH)_2$	Mesoporous	318	\	85 % (0.5 A g^{-1}, 500 cycles)	\	9
α-$Ni(OH)_2$	Flowerlike	72.9	\	77.9 % (50 mV s^{-1} 2000 cycles)	\	10
α-$Ni(OH)_2$	Microflowers	185	\	90 % (1000 cycles)	\	11
α-$Ni(OH)_2$ mixed with β-$Ni(OH)_2$	nanosheet	\	\	91 % (10 A g^{-1}, 500 cycles)	3-4 mg	12
Amorphous $Ni(OH)_2$	hollow nanobox	214.6	\	95 % (5 A g^{-1} 1200 cycles)	1~2 mg	13
Amorphous $Ni(OH)_2$	nanosphere	\	\	81 % (100 mV s^{-1} 10000 cycles)	0.12 mg	14
$NiCo_2O_4$ array	hierarchical superstructure	36.7	348.9 (1 A g^{-1}) ~340 (2 A g^{-1}) 325.9 (5 A g^{-1}) ~310 (10 A g^{-1}) ~295 (15 A g^{-1})	93.6 % (10 A g^{-1}, 3000 cycles)	\	15

Table S2 Literature comparison of supercapacitor performance based on $Co(OH)_2$. In particular, papers reporting powder-based α-$Co(OH)_2$ are exhaustively collected. The parameters which are superior, comparable or inferior to those of LP α-$Co(OH)_2$ are highlighted as blue, green or red, respectively.

Phase	Structure	Specific surface area / $m^2\ g^{-1}$	Specific capacity (C g^{-1})	Cycling retention	Loading mass / mg	Refs.
α-$Co(OH)_2$	**Loosely packed**	**72.0**	**578.0 (1 A g^{-1})** **553.8 (2 A g^{-1})** **486.5 (5 A g^{-1})** **432.0 (10 A g^{-1})** **360.0 (20 A g^{-1})**	**72.4 % (10 A g-1 5000 cyckes)**	**1.5 ± 0.3**	**This work**
α-$Co(OH)_2$	**Well developed sheets**	**34.9**	**405.4 (1 A g^{-1})** **396.0 (2 A g^{-1})** **339.0 (5 A g^{-1})** **305.0 (10 A g^{-1})** **264.0 (20 A g^{-1})**	**74.5 % (10 A g^{-1} 5000 cycles)**	**1.5 ± 0.3**	**This work**
α-$Co(OH)_2$	Cl^- intercalated, sheet and cluster	\	\	73 % (3 A g^{-1}, 100 cycles)	\	16
α-$Co(OH)_2$	nanosheet	\	\	72.8 % (2 A g^{-1}, 2000 cycles)	2.0	17
α-$Co(OH)_2$	Exfoliated layers	97.2	\	no obvious decay (0.5~2.5 A g^{-1}, 5000 cycles)	10	18
α-$Co(OH)_2$	nanosheets	\	\	98 % (4 A g^{-1} 1000 cycles)	7.5	19
β-$Co(OH)_2$	Porous	190.2	\	93 % (1A g^{-1}, 500 cycles)	\	20
β-$Co(OH)_2$	nanoplates	104	\	92 % (2 A g^{-1}, 1000 cycle)	25 mg	21
β-$Co(OH)_2$	mesoporous	400.4	\	96 % (1 A g^{-1}, 1000 cycle)	\	22

1. G. J. d. A. A. Soler-Illia, M. Jobbágy, A. E. Regazzoni and M. A. Blesa, *Chem. Mater.*, 1999, **11**, 3140-3146.
2. J. Nai, J. Wu, L. Guo and S. Yang, *Crystal Growth & Design*, 2012, **12**, 2653-2661.
3. R. Demichelis, P. Raiteri, J. D. Gale, D. Quigley and D. Gebauer, *Nat Commun*, 2011, **2**, 590.
4. W. J. E. M. Habraken, J. Tao, L. J. Brylka, H. Friedrich, L. Bertinetti, A. S. Schenk, A. Verch, V. Dmitrovic, P. H. H. Bomans, P. M. Frederik, J. Laven, P. van der Schoot, B. Aichmayer, G. de With, J. J. DeYoreo and N. A. J. M. Sommerdijk, *Nat Commun*, 2013, **4**, 1507.
5. D. Gebauer, A. Völkel and H. Cölfen, *Science*, 2008, **322**, 1819-1822.
6. H.-P. Cong, X.-C. Ren, P. Wang and S.-H. Yu, *ACS Nano*, 2012, **6**, 2693-2703.
7. Y. Xu, K. Sheng, C. Li and G. Shi, *ACS Nano*, 2010, **4**, 4324-4330.
8. K. Wang and L. Zhang, *Electrochemistry*, 2013, **81**, 259-261.
9. H. Du, L. Jiao, K. Cao, Y. Wang and H. Yuan, *ACS Appl. Mater. Interfaces*, 2013, **5**, 6643-6648.
10. H. Jiang, T. Zhao, C. Li and J. Ma, *J. Mater. Chem.*, 2011, **21**, 3818-3823.
11. B. P. Bastakoti, H.-S. Huang, L.-C. Chen, K. C.-W. Wu and Y. Yamauchi, *Chem. Commun.*, 2012, **48**, 9150-9152.
12. P. Lu, F. Liu, D. Xue, H. Yang and Y. Liu, *Electrochim. Acta*, 2012, **78**, 1-10.
13. Y. Fu, J. Song, Y. Zhu and C. Cao, *J. Power Sources*, 2014, **262**, 344-348.
14. H. B. Li, M. H. Yu, F. X. Wang, P. Liu, Y. Liang, J. Xiao, C. X. Wang, Y. X. Tong and G. W. Yang, *Nat Commun*, 2013, **4**, 1894.
15. Q. Zhou, X. Wang, Y. Liu, Y. He, Y. Gao and J. Liu, *J. Electrochem. Soc.*, 2014, **161**, A1922-A1926.
16. Z.-A. Hu, Y.-L. Xie, Y.-X. Wang, L.-J. Xie, G.-R. Fu, X.-Q. Jin, Z.-Y. Zhang, Y.-Y. Yang and H.-Y. Wu, *J. Phys. Chem. C*, 2009, **113**, 12502-12508.
17. X. Ge, C. D. Gu, X. L. Wang and J. P. Tu, *J. Phys. Chem. C*, 2014,

118, 911-923.
18. Z. Gao, W. Yang, Y. Yan, J. Wang, J. Ma, X. Zhang, B. Xing and L. Liu, *Eur. J. Inorg. Chem.*, 2013, **2013**, 4832-4838.
19. T. Wu and C. Yuan, *Mater. Lett.*, 2012, **85**, 161-163.
20. C. Mondal, M. Ganguly, P. K. Manna, S. Yusuf and T. Pal, *Langmuir*, 2013, **29**, 9179-9187.
21. M. Aghazadeh, S. Dalvand and M. Hosseinifard, *Ceram. Int.*, 2014, **40**, 3485-3493.
22. B. G. Choi, M. Yang, S. C. Jung, K. G. Lee, J.-G. Kim, H. Park, T. J. Park, S. B. Lee, Y.-K. Han and Y. S. Huh, *ACS Nano*, 2013, **7**, 2453-2460.